Eur Biophys J (2009) 38:961–970
DOI 10.1007/s00249-009-0476-3

ORIGINAL PAPER

Computational study of the transmembrane domain of the acetylcholine receptor

Chen Song · Ben Corry

Received: 24 December 2008 / Revised: 1 May 2009 / Accepted: 4 May 2009 / Published online: 23 May 2009
© European Biophysical Societies' Association 2009

Abstract The nicotinic acetylcholine receptor (nAChR) is a ligand-gated ion channel protein whose transmembrane domain (TM-domain) is believed to be responsible for channel gating via a hydrophobic effect. In this work, we perform molecular dynamics and Brownian dynamics simulations to investigate the effect of transmembrane potential on the conformation and water occupancy of TM-domain, and the resulting ion permeation events. The results show that the behavior of the hydrophobic gate is voltage-dependent. Large hyperpolarized membrane potential can change the conformation of TM-domain and water occupancy in this region, which may enable ion conduction. An electrostatic gating mechanism is also proposed from our simulations, which seems to play a role in addition to the well-known hydrophobic effect.

Keywords Ion channel · Acetylcholine receptor · Gating · Membrane potential · Molecular dynamics · Brownian dynamics

Introduction

The nicotinic acetylcholine receptor (nAChR) belongs to the "Cys-loop" family of ligand-gated ion channels that mediate synaptic neurotransmission (Sine and Engel 2006). The nAChR is of crucial physiological importance and its malfunction is related to a number of known diseases including epilepsy, congenital myasthenia, and muscle weakness (Ashcroft 2006). However, although the genetics, kinetics, electrophysiology, and many topological aspects have been well characterized for the nAChR (Barry and Lynch 2005; Jordan 2005), an atomic-scale understanding of the protein was not available until the development of recent models based on 4-Å-resolution maps obtained from cryo-electron microscopy (Miyazawa et al. 2003; Unwin 2005). The channel is made up of five homologous subunits packed around a central pore, forming a structure with five-fold pseudosymmetry. It is divided into three domains, including the transmembrane domain (TM-domain), which is embedded in the lipid as shown in Fig. 1 and is believed to be responsible for the gating behavior.

Since the appearance of experimentally based models of the *Torpedo* nAChR (Miyazawa et al. 2003; Unwin 2005), much theoretical research has taken place to study where and how the gating mechanism happens in the TM-domain (Cheng et al. 2006; Corry 2004, 2006; Law et al. 2005; Taly et al. 2005). While there has been some suggestion that the channel gate is located at the intracellular end of the TM-domain at the location of a number of charged or polar residues (Pascual and Karlin 1998; Wilson and Karlin 1998), a more common view is developing that the gate is midway across the membrane. Here there are a number of hydrophobic residues that may act to block ion permeation using a so-called hydrophobic gating mechanism by which a closed-state pore is not necessary physically blocked, and a small radius change can dramatically improve the water occupancy, which may lead to ion conduction (Beckstein et al. 2003; Beckstein and Sansom 2006; Corry 2006; Cymes and Grosman 2008). As yet, this has not been shown to occur in the more recent refined structure of nAChR (Unwin 2005). However, the gating mechanism is still not clear due to the lack of dynamic gating details and

C. Song (✉) · B. Corry
School of Biomedical, Biomolecular and Chemical Sciences,
The University of Western Australia,
Crawley, WA 6009, Australia
e-mail: sc3210@gmail.com

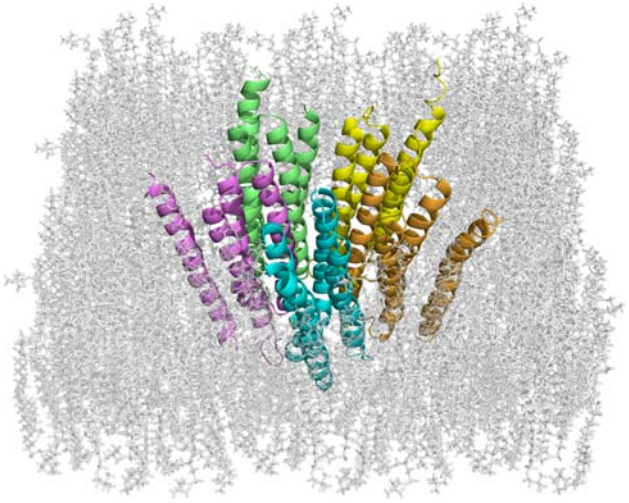

Fig. 1 The TM-domain of the refined cryo-electron microscopy structure of nAChR, embedded in lipid membrane. The five subunits are indicated with different colors

limitations of the molecular dynamics (MD) simulation time scale. The very recent X-ray structures of the closed-state (Hilf and Dutzler 2008) and the "apparently" open-state pentameric ligand-gated ion channel proteins (Bocquet et al. 2009; Hilf and Dutzler 2009) have provided more information on the gating mechanism. But more research is needed to examine if this is a common feature of all the Cys-loop family. In addition, there are still some relevant issues unresolved. For example, some experimental results indicate that the gating behavior of nAChR may be voltage-dependent (Auerbach et al. 1996; Chabala 1992), but the influence of the membrane potential on the conformation of the protein remains unclear. Recent theoretical studies have shown that membrane potential may change the hydrophobic properties of a similar pore (MscS) (Sotomayor et al. 2007; Spronk et al. 2006). Of more direct interest, Wang et al. have witnessed an ion permeation event in MD simulations of a homology model of nAChR at physiological and hyperpolarized membrane potentials (Wang et al. 2008). Thus, it is of interest to investigate the effect of voltage on the pore conformation, water occupancy in the pore, and ion conduction properties of nAChR in more detail.

In this work, we perform MD simulations to investigate the effect that a large membrane potential can have on the conformation and water occupancy in the TM-domain of nAChR. Brownian dynamics (BD) simulations are also carried out to investigate the ion permeation events. Our studies indicate that the membrane potential does affect the gating behavior of the TM-domain, and an electrostatic effect may also play a role in the gating behavior of the nAChR in addition to the "hydrophobic" gating mechanism.

Methods

MD simulations

MD simulations were performed starting with the TM-domain of the refined structure of the nAChR (Protein Data Bank entry 2BG9) (Unwin 2005). The TM-domain was chosen by selecting residues from the α-subunit along with residues with a corresponding range of z coordinates from the other subunits. Residues P211-H306 and K400-G437 of the α-subunit were selected.

Before performing MD simulations on the TM-domain, we placed it within a POPC lipid membrane (as shown in Fig. 1) and solvated the system with the TIP3 water molecules, to which we added 26 Cl^- and 25 Na^+ ions to get a neutral system, resulting in a $117 \times 117 \times 83$ $Å^3$ water box with about 0.15 M ion concentration (105,720 atoms altogether). The lipid and water were initially energy minimized for 50,000 steps and equilibrated for 20 ps with the protein held fixed. Then harmonic constraints were applied to the α-carbon atoms of the protein, and a further 5,000 steps of energy minimization and 20 ps of equilibration were performed. Finally all constraints were released, and the system was energy minimized for 5,000 steps and 60 ps of simulation was conducted before data collection began. After a 5-ns MD simulation of the TM-domain, we saved the system coordinates to use as the initial structure of the subsequent simulations. Here we performed another two 4-ns MD simulations with external applied electric fields of +100 and −100 mV/nm (positive direction is pointing from the intracellular entrance to the extracellular entrance, along the channel axis) across the protein-membrane system. Note that here we adopted an extremely large electric field in order to find appreciable changes within the available MD time scale.

The MD simulations were performed using periodic boundary conditions with the NAMD2 program (Phillips et al. 2005) using the CHARMM27 force field (MacKerell et al. 1998). A short-range cutoff of 12 Å was used for nonbonded interactions, and the long-range electrostatic interactions were calculated with particle mesh Ewald method (Darden et al. 1993; Essmann et al. 1995). Langevin dynamics and a Langevin piston algorithm were used to maintain the temperature at 310 K and the pressure at 1 atm. The time step was set to 1 fs.

We did not consider any alternative bilayer compositions in this study although they were also available, since adopting POPC made our study more consistent with most of the previous simulation studies.

BD simulations

Ion conduction events were simulated explicitly using BD simulations, which have been successfully applied to the

nAChR and other channels (Corry 2006; Corry et al. 2001). The motion of individual ions is traced explicitly, but the water and protein atoms are treated as continuous dielectric media (Chung et al. 2002; Li et al. 1998). The channel is taken to be a rigid structure during the simulation, and partial charges are assigned to the protein using the CHARMM all-atom parameter set. A number of Na^+ and Cl^- ions are placed in cylindrical reservoirs of radius 30 Å at each end of the channel that mimic the intra- and extracellular solution, and the height of the cylinder is adjusted to bring the solution to the desired concentration. The motion of these ions under the influence of electric and random forces is then traced using the Langevin equation. The total force acting on each ion in the assembly is calculated, and then new positions are determined for the ions a short time later. Electrostatic forces are calculated by assigning dielectric constants of 2 to the protein and 60 to the water in the channel and solving Poisson's equation using an iterative method (Hoyles et al. 1998). [These dielectric constants were established to give the best agreement with experimental results of previous studies (Chung et al. 1999; Corry et al. 2004; Ng et al. 2008; O'Mara et al. 2005)]. The current is determined directly from the number of ions passing through the channel.

BD simulations were performed for TM-domain under different transmembrane voltages. When calculating currents for the TM-domain, we used the average structures taken from the last 1 ns of the three corresponding MD simulations of the TM-domain as the fixed protein structures and applied 0, ±50 and ±100 mV/nm electric fields to the BD simulations.

Results and discussion

First, we performed MD simulation for the TM-domain without an external field according to the method described above (marked as TM1). The evolution of the root-mean-squared deviation (RMSD) of the protein (calculated only for non-hydrogen atoms) is shown in Fig. 2a by the black line. As can be seen, the simulation reaches a stable stage after 2 ns of simulation, with an average RMSD value of about 3.25 Å, showing that the experimental structure is relatively stable under our simulation protocol. After applying the −100 (marked as TM2) and +100 (marked as TM3) mV/nm external electric field at the end of the 5-ns simulation, the conformation is further changed. As shown in Fig. 2a with red and blue lines, this change occurs rapidly at the start of the simulation, before continuing gradually over the latter part of the 4-ns simulations. Without doubt, the external electric field alters the conformation of the TM-domain.

To examine how the pore is influenced by the applied electric field, we calculated the average structure in the last nanosecond for each of the simulations TM1, TM2, and TM3, and then calculated their pore radii as plotted in Fig. 2b. Here the black line is the radius for the average structure of the simulation TM1, while the red and blue lines are those for TM2 and TM3, respectively. We can see that as a result of applying a negative electric field, the pore radius is significantly changed (red line), with the minimum

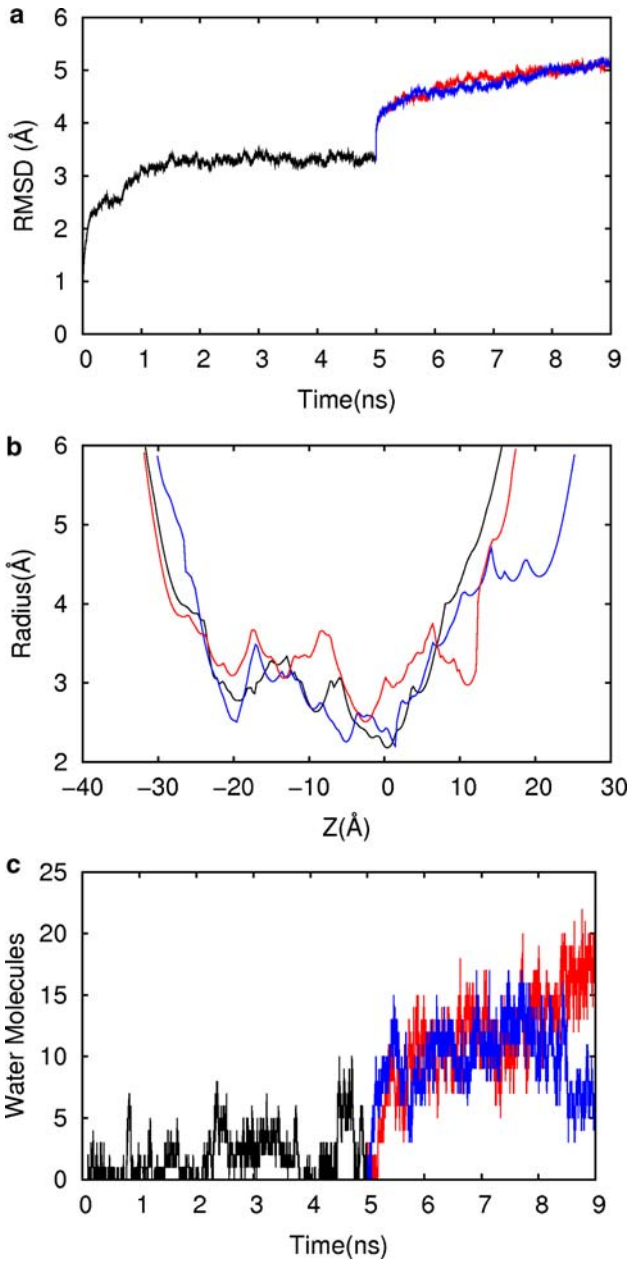

Fig. 2 Simulations of the TM-domain. **a** Evolution of the RMSD from the starting structure for MD simulations of the TM-domain before and after the application of an electric field. **b** The pore radii of the average structure in the last nanosecond of each simulation. **c** The number of water molecules in the hydrophobic region of the TM-domain during the three simulations. TM1 (no applied field) in *black*, TM2 (−100 mV/nm) in *red*, and TM3 (+100 mV/nm) in *blue*

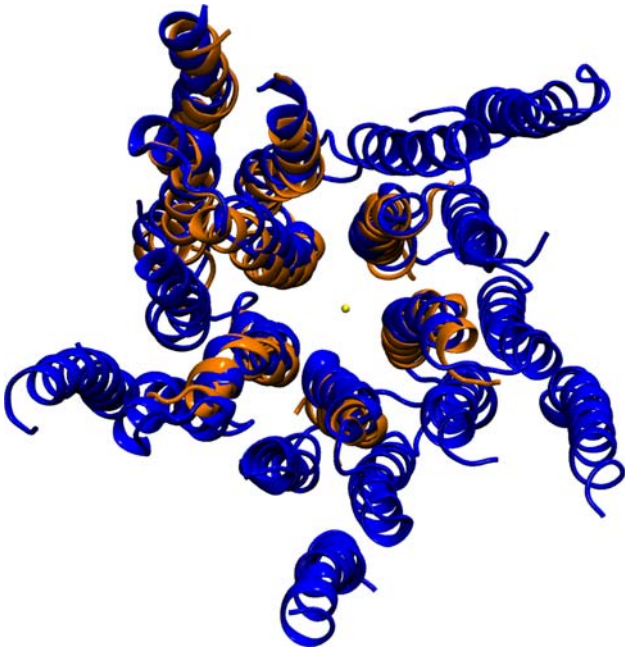

Fig. 3 Conformation changes of TM-domain induced by the application of the negative electric field. The *blue helices* indicate the average structure of the TM-domain for the simulation without external electric field, while the *orange* is that of the simulation with −100 mV/nm electric field. For clarity, only the M2 helix is shown for four subunits, and the center of the pore is indicated

radius increasing by about 0.5 Å. This is particularly interesting as previous simulations have suggested that such a radius change may be all that is required to alter the pore from being nonconductive to conductive (Beckstein and Sansom 2004; Corry 2006).

Careful examination of the average structures shows that after applying the negative electric field, the inner ring of helices (M2) tilts to widen the intracellular end of the channel, and slightly rotates counterclockwise ∼5° about the axis of the pore (looking from the extracellular direction) as indicated in Fig. 3. Under a positive electric field, the change in pore radius is less dramatic, and the minimum radius is quite similar to that without the electric field.

It is interesting to note that the rotation of M2 under the negative electric field is similar to that suggested previously to be involved in channel opening (Corry 2006; Unwin 1995, 2003), albeit to a smaller extent. Although huge electric fields were applied during our simulations, we do find interesting motions of M2 that are consistent with previous hypotheses. Liu et al. also noticed a local bending and rotation in a conventional molecular dynamics simulation for the closed-state structure (Liu et al. 2008), which is consistent with what we found when applying a negative electric field. All these results indicate that both tilting and rotation movements of M2 helices may be related to the opening of the channel. A negative voltage can induce more dramatic changes in the radius and conformations of TM-domain than positive voltage. Unfortunately, no quantitative description can be given here about how conformation changes under realistic physiological conditions, i.e., when transmembrane potential exists across membranes. We suppose a similar but more minor effect could occur.

Previous studies have shown that there is a hydrophobic girdle in the TM-domain, which is believed to be responsible for the "hydrophobic" gating mechanism (Beckstein and Sansom 2006; Corry 2006). In our simulations, we also found that this hydrophobic region, which extends from L251 to V259 of the α subunit, restricts water occupancy in the pore and is therefore likely to prevent the passage of ions. More interestingly, after applying the external field, the water occupancy in the hydrophobic region is enhanced, as shown in Fig. 2c. Without an applied field there are about 2.5 water molecules located in the hydrophobic region on average, and much of the time no water molecules reside in this ca. 8-Å-long region. After applying the external field, the number of water molecules was dramatically increased in a short time in both the +100 and −100 mV/nm situations. This is similar to previous studies of the mechanosensitive channel MscS, which also indicate that the water occupancy in the hydrophobic channel pore is voltage dependent (Sotomayor et al. 2007; Spronk et al. 2006). In our case we do see differing behavior under positive and negative fields. For the case of a positive electric field, the number of water molecules fluctuates after increasing to stable values of about 10.3 and then slightly drops in the last nanosecond, while for the negative electric field case, the number of water molecules keeps increasing during the entire 4-ns MD simulation.

To give an overall description of the water distribution in the whole TM-domain, we calculated the average water densities of the last nanosecond of the TM1, TM2, and TM3 simulations, as shown with slices in Fig. 4. It is very obvious that when there is no external electric field, there is a hydrophobic region in the TM-domain with decreased water density that is occupied with more water molecules after an electric field is applied. For the TM2 (negative electric field) simulation, the pore is almost fully hydrated, which may be due to the wider pore radius since previous studies have shown that a small increase in radius can lead to an obvious enhancement in water occupancy (Beckstein et al. 2003). It is notable that the applied field can also increase water occupancy without increasing the pore radius as under a positive electric field.

We have also examined how the water molecules orient in the pore during the simulations. Three typical snapshots are shown in Fig. 5. As can be seen, before applying any electric field, water molecules do not have any obvious orientation, and it is hard for water molecules to reside across the hydrophobic region. After applying a negative electric

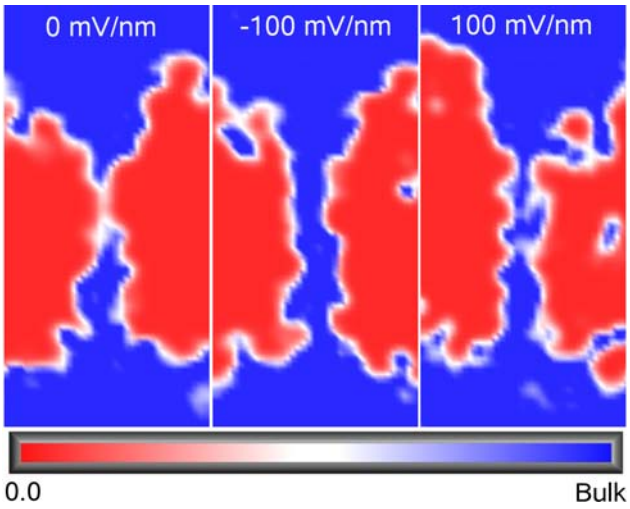

Fig. 4 Water density in the TM-domain. The average density of water in a central slice through the pore during simulations of the TM-domain calculated from the last nanosecond of the three simulations. The *left panel* is for TM1, *middle* for TM2, and *right* for TM3. The *blue color* corresponds to bulk water density, and *red* to total absence of water

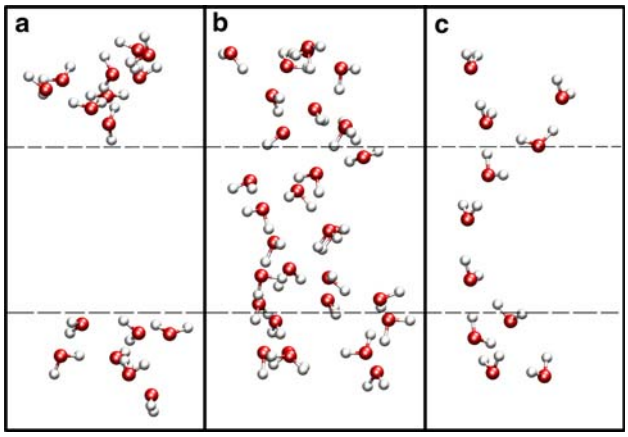

Fig. 5 Water distribution around the hydrophobic region in the TM pore from a snapshot of **a** TM1, **b** TM2, and **c** TM3 simulations. The edges of the hydrophobic regions are marked with *dashed lines*

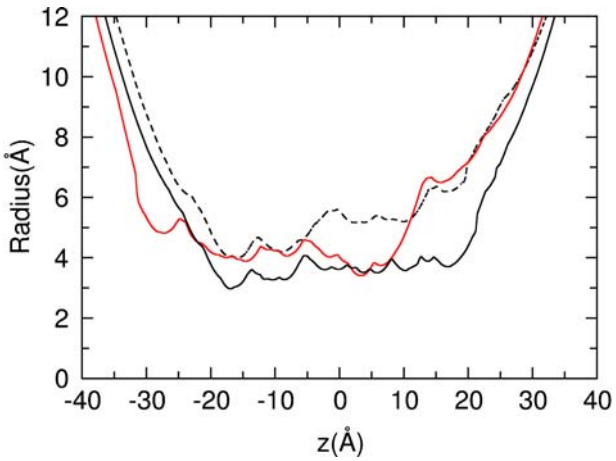

Fig. 6 Pore radius of the TM-domain of the putative open structure. The pore radii of the initial putative structure (*black dashed line*), the final structure after 10-ns MD simulations without external electric field (*black solid line*), and the final structure of 10-ns MD simulations with −100 mV/nm field (*red line*), starting from the putative structure, are shown

field, water molecules are seen to have a well-defined orientation along the direction of the electric field as shown in Fig. 5b, due to the intrinsic polarity of water molecules. A similar situation takes place when applying a positive electric field as shown in Fig. 5c. Since there is a widening of the pore when applying a negative electric field (Fig. 2b), more water molecules are able to get into the pore than under a positive electric field. However, because the applied electric field can still assist water molecules to form a single-file chain structure with well-arranged orientation, which is favorable in narrow channels as shown by previous studies (Hummer et al. 2001), water molecules are also able to permeate through the channel under a positive electric field, although no widening of the pore is found in this case. Therefore, the external electric field can not only help to change the conformation of the pore but also assist water molecules to arrange their orientations, which will favor their occupancy and permeation across the hydrophobic region. In the case of nAChR, the negative electric field does have a larger effect on the conformation of the pore, which results in more water molecules getting into the hydrophobic region.

To further validate the hypothesis that negative voltage might assist opening of the pore or keeping the pore open, we performed two additional 10-ns simulations on the putative open structure as proposed in one of our previous studies (Corry 2006). The putative open structure was obtained by rotating the inner M2 helix of each of the five subunits clockwise by 15° about the axis passing perpendicular to the membrane through the disulphide bridge of the binding domain. Then the intracellular end of the helix is rotated counterclockwise by 30° to produce a slight kink. The net effect of this conformational change is to widen the pore by ~1.5 Å. MD simulations were performed starting from this putative open structure, both without external electric field and with −100 mV/nm. The pore radii at the end of the simulations are shown in Fig. 6. As can be seen, if there is no external field across the membrane, the pore radius significantly shrinks (1–2 Å) within 10 ns. However, when the −100 mV/nm electric field is applied, the radius of the putative open structure does not change so much. Although the minimum radius also drops, the change occurs only locally around $z = 4$ Å, while most of the other part did not change much, which means that the negative electric field does help to keep the pore open.

Our MD simulations shed further light on the kinetics of nAChR gating. While previous physiological studies

suggest hyperpolarization makes the open state of the pore more likely, there are some contradictions regarding whether the opening rate or closing rate of the channel is most sensitive to the change in potential. Although earlier studies show that only the closing rate decreases with the hyperpolarization (Liu and Dilger 1991; Magleby and Stevens 1972; Sheridan and Lester 1977), there are also some other studies showing the opening rate also increases with the hyperpolarization (Chabala 1992; Leibowitz and Dionne 1984). More recent studies showed that, for the diliganded nAChR, the closing rate decreases with the hyperpolarization (Auerbach et al. 1996), while for the unliganded nAChR, the opening rate increases with the hyperpolarization (Grosman and Auerbach 2000; Jackson 1986).

In our MD simulations under negative voltage, not only was the accelerated opening of the pore observed from the simulation starting with the closed-state structure, but also the slowed closing of the pore was witnessed from the MD simulation starting with the putative open structure, which means that both the closing rate and opening rate might be voltage dependent. The microscopic mechanism responsible for this might come from two factors. One is that the hyperpolarization potential may directly destabilize the conformation of the closed state and help the pore open. The other is that the hyperpolarized potential may assist the water molecules to form an orientated arrangement and enter the pore, which breaks the hydrophobic girdle closing the pore. Either of these factors could act to increase the channel opening rate or decrease the closing rate. It is plausible from our studies, therefore, that either could be voltage dependent. Regardless of the mechanism, our computational study supports the previous experimental conclusion that a hyperpolarized potential will shift the equilibrium constant in favor of the open state.

Since external electric fields have changed the conformation of the TM-domain and the pore radius, it is interesting to explore whether it is possible for ions to pass through. Using the average structures of the last nanosecond of the simulations TM1, TM2, and TM3, we performed BD simulations with the external electric fields of 0 and ±100 mV/nm for the TM1 conformation and 0, ±50, and ±100 mV/nm for the TM2 and TM3 conformations. The BD results show that ions can conduct only in the BD simulation with electric field of ±100 mV/nm on the TM2 conformation. In the case of −100 mV/nm, it was seen that about 77 Na^+ ions passed downwards within 0.2 μs, which is approximately −61.7 pA under the voltage of −400 mV crossing over the TM-domain. In the case of 100 mV/nm across the TM2 conformation, there were about 7.5 Na^+ passing upwards on average within 0.2 μs. However, there was no current found in any other cases. These results indicate that both a negative transmembrane potential and an induced conformation rearrangement are necessary for ion permeation, since no ion can permeate in the BD simulation with −100 mV/nm field for the TM1 conformation. We should keep it in mind that, although the pore radius has been widened due to the large negative field, the protein structure is obtained from the closed-state structure, and we do not expect the final structure to represent a fully open state. Thus, the current observed here is likely to partially result from the extremely large electric field, which may introduce some artifact. However, considering the fact that no similar current takes place in the case of TM1 or TM3 conformation, we can still extract some information from these results, i.e., negative membrane potential can affect the ion conduction and conformation of the TM-domain. As none of our simulations were conducted on the open state of the pore, our results do not imply that the open state of the channel would display rectification. Negative potentials may, however, assist in opening or keeping open the pore more than positive ones. This could be expected to reveal itself in increases in the channel opening rate constant or decreases in the channel closing rate constant under hyperpolarization in partial agreement with previous experimental observations.

We have also noted a recent study by Wang et al. in which they investigated the effect of membrane potential on the cation permeation through the human adult muscle nAChR (Wang et al. 2008). Despite studying a different homology model and adopting different simulation methods, they also found cations can permeate through the channel under external electric potential. Thus, analogous results have been obtained for both the *Torpedo* structure and the homology model of human adult-type muscle nAChR, which confirms the concept that membrane potential can play a role in channel gating and ion permeation in ligand-gated ion channels. Furthermore, both works indicate that Unwin's 2BG9 model is indeed an inactive model, since no ion permeation was seen in the BD simulations on the protein conformation obtained in the absence of an electric field even under large membrane potentials in our work, or in the MD simulation of the restrained homology models of 2BG9 in the work of Wang et al. In both cases, cation permeation could only be obtained after an induced conformational change. It is also notable that, although in our simulations, extracellular and intracellular domains of the nAChR were absent, consistent results were obtained with those from Wang et al.'s work.

To give a more detailed analysis of the effect of hyperpolarized membrane potential on the ion conduction events, we analyzed the ion conduction trajectory of the BD simulations and found some interesting results. We counted the dwell time of Na^+ in the channel of TM-domain during the BD simulation for the TM2 conformation under −100 mV/nm electrostatic field. The result is shown in Fig. 7a. As can

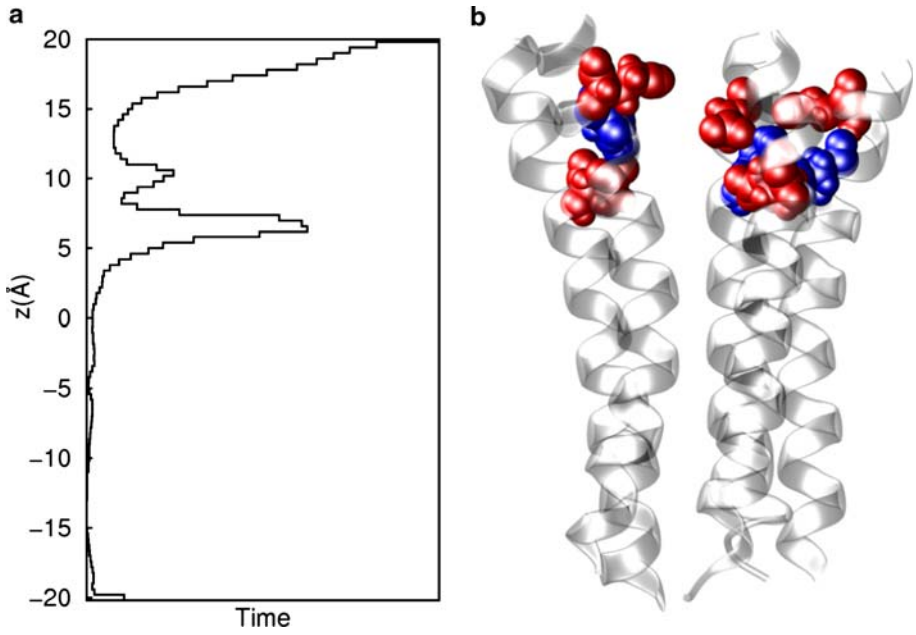

Fig. 7 **a** The relative dwell time of Na^+ in the TM-domain. **b** The Glu, Lys, and Arg residues at the extracellular entrance of M2 helices. The Glu residues are shown with *red spheres*, and Lys and Arg with *blue ones*

be seen, the locations where Na^+ ions dwell longest are at $z \approx 20$ Å, which is just at the entrance of the pore, and at $z \approx 6$ Å, which is just before the narrowest hydrophobic region in the middle of the channel. This is consistent with the hydrophobic gate position and thus confirms the gate position again. Furthermore, we found that there was an electrostatic potential well around this region, mainly due to the presence of more glutamic acids than lysines and arginines in the M2 helices, i.e., 5 Glu versus 3 Lys + Arg as shown in Fig. 7b. Therefore, one may question whether electrostatic effects of these charged residues can contribute to channel gating in addition to the hydrophobic mechanism.

To address this question, we calculated the potential energy profiles for one Na^+ to permeate along the channel axis. Four situations were considered: TM1 conformation with 0 and −100 mV/nm, and TM2 conformation with 0 and −100 mV/nm. The results are shown in Fig. 8a with solid lines. It is quite obvious that there are energy wells around the extracellular entrance ($z \approx 15$ Å) for all cases, created by the acidic residues in this region. For the case of TM1 conformation without external electric field, there is an energy barrier of ∼24.1 kcal/mol for one Na^+ to permeate as shown with the black line in Fig. 8a. For the case of TM2 conformation without external electric field, the barrier was reduced to ∼13.9 kcal/mol as shown with a blue line, which means that the conformation change alone (widening of the radius about 0.5 Å) can dramatically reduce the potential energy barrier for one Na^+ to pass by 10.3 kcal/mol.

If we look at the case of TM1 conformation with −100 mV/nm external electric field as shown with the red line, we can see an energy barrier of ∼8.1 kcal/mol, while for the case of TM2 conformation with −100 mV/nm (green line), the energy barrier was again reduced to ∼2.7 kcal/mol. Therefore, from Fig. 8a, we can clearly see that the widening of the pore can reduce the potential energy barrier for ions to pass through the hydrophobic region of the pore by both increasing the width of the hydrophobic girdle and weakening the attraction of the acidic residues by moving them farther from the pore axis. To analyze the importance of each of these effects in reducing the barrier to ion permeation, we decomposed the change in energy barrier between the TM1 and TM2 conformations. To do this, we determined the energy barriers to ion permeation coming from the electrostatic interactions alone, i.e., not including image charges created by the ion or desolvation effects that comprise the so-called hydrophobic barrier.

The electrostatic potential energy profiles for a test Na^+ to move along the pore axis determined this way for the conformations TM1 and TM2 without any external electric field are shown with dashed lines in Fig. 8a. The energy barriers for those two cases are 17.5 and 11.4 kcal/mol, respectively. Therefore, of the total reduction in the potential energy barrier to ion permeation created by widening the pore, 6 kcal/mol (or ∼60%) is due to the changing electrostatic interactions of the ion with the protein caused by a weakened attraction to the acidic residues at the external end of the pore. The remaining 4 kcal/mol (∼40%) is due to the lesser hydrophobic barrier that results from widening the nonpolar constriction. Our results suggest that an electrostatic effect can also play an important role in the gating of the nAChR in addition to the well-known hydrophobic effect.

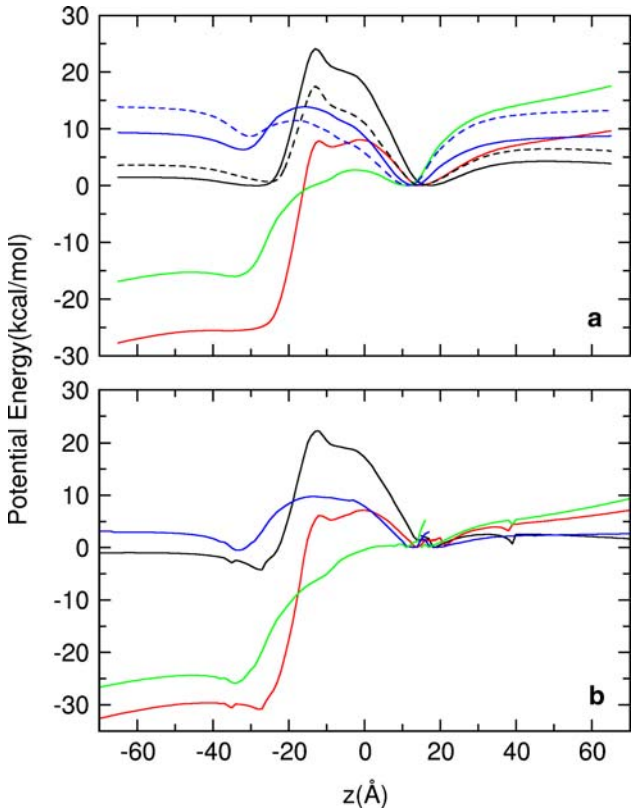

Fig. 8 Potential energy of Na^+ moving through the pore. **a** The single-ion potential energy (*solid lines*) calculated by moving one Na^+ through the pore, and the single-ion electrostatic potential energy (*dashed lines*) where only the electrostatic interaction between the test ion and the protein was considered. **b** The two-ion potential energy, calculated by moving one ion through the pore while another resides in the energy well inside the extracellular end of the pore. In each case, the TM1 conformation with 0 mV/nm is in *black*, the TM1 conformation with −100 mV/nm is in *red*, the TM2 conformation with 0 mV/nm is in *blue*, and TM2 conformation with −100 mV/nm is in *green*

Although the wider pore in the TM2 conformation reduces the energy barrier for ion permeation, we note from Fig. 8a that a significant barrier (∼2.7 kcal/mol) remains even under a large applied field that would prevent any significant ion current in contrast to what is seen in the BD simulations. In fact, when we examined the BD simulation trajectories, an interesting feature was noted. We found that the Na^+ permeation events involve multiple ions and can be divided into three stages: (1) One Na^+ comes into the extracellular entrance and fluctuates around but can not pass, as shown in Fig. 9a. (2) Another Na^+ comes into the entrance and fluctuates as well, together with the first Na^+, as shown in Fig. 9b. (3) After some time, the first Na^+ passes through the channel rapidly as shown in Fig. 9c, which returns the system back to step one. This is a common feature in most of the Na^+ permeation events in our BD simulations, which highlights the importance of the occupancy of multiple cations at the extracellular entrance of the channel and the intercation Coulombic repulsion.

To account for this, we reexamined the potential energy barriers for Na^+ to permeate, taking into account the effect of the second ion. To do this we calculated the two-ion potential energy profiles for the four cases described above. When doing this, one Na^+ was put around the location of the minima in the single ion profile ($z = 14$), and the potential energy for another Na^+ was calculated as it was moved from $z = 70$ to $z = 15$, while the first ion was allowed to find its minimum energy position. Then, one Na^+ was put at $z = 18$, and the potential energy for the other Na^+ was calculated from $z = 17$ to $z = -70$. The combination of these two results gives a description of the potential energy along the pore axis including the multi-ion nature of conduction. All the results are shown in Fig. 8b. As can be seen, the most distinct difference compared to Fig. 8a is that all the energy barriers are reduced. In particular, there is only a very small energy barrier (∼0.25 kcal/mol) for Na^+ to pass in the TM2 conformation with −100 mV/nm external electric field, which is also the reason why we can find a large current in this case. These results indicate that the conduction of Na^+ is a two-ion process, as also witnessed by the trajectory analysis, i.e., the occupancy of the second Na^+ in the extracellular entrance of TM-domain is essential for the first Na^+ to permeate.

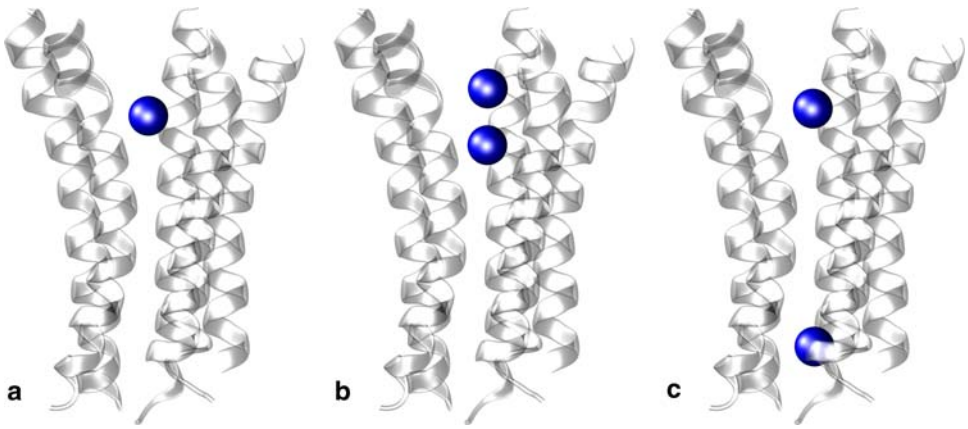

Fig. 9 The ion permeation process in the channel. **a** One Na^+ comes into the extracellular entrance, **b** a second Na^+ comes in as well, and **c** the first Na^+ passes through. For clarity, only the M2 helices are shown here

The multi-ion conduction mechanism seen here shares some similarities with that found by Wang et al. in their MD simulations. In their case, only one Na^+ was seen in the TM-domain. However, they found that intercation Coulombic repulsion is still important, although the second ion remains farther away from the TM domain and only enters when the first ion has passed through the channel. Thus, the differences seem only to lie in the exact position of the second Na^+ ion. One drawback of our simulation is that the extracellular and intracellular domains of the nAChR are not included, which may affect the conformation of the TM-domain. But this will not affect the general electrostatic gating idea, and Wang et al.'s work has already shown similar MD results, where all the three domains were included, which can be viewed as support for our conclusion. It should also be noted that we do not account for the flexibility of the protein, as the structure was fixed in the BD simulation. This is also one of the reasons why we have to apply a larger transmembrane potential to see the ion permeation events.

Summary

In this study, we performed MD and BD simulations on the TM-domain of nAChR to further explore its gating behavior. Our results on the refined structure support previous studies on earlier structural models that suggest the hydrophobic region in the center of the TM-domain is probably the channel gate that determines whether ions can conduct. Notably, we find that an external voltage, especially negative voltage, can change the conformation and water occupancy at the hydrophobic region of the TM-domain, which can assist in opening or holding open the pore. This could either be due to a direct force upon the protein, or by assisting the entry of water into the pore, breaking the hydrophobic girdle. An increase in water occupancy can also occur without a significant conformational change under an applied field.

BD simulations also confirm that the gating position is around the middle hydrophobic region and there is also an electrostatic potential energy barrier in this region. In conjunction with electrostatic potential energy calculations, the simulations indicate that the widening of the pore can reduce the barrier to ion permeation. Rather than simply being a consequence of reducing the desolvation barrier (hydrophobic gating), we show that much of this is due to a weakening of the electrostatic attraction of the acidic residues at the channel mouth. This result implies that an electrostatic effect can also play a role in the gating mechanism in addition to the well-known hydrophobic effect. This electrostatic gating can occur in nonoccluded pores and could be a common feature in controlling ion permeation in narrow channels. BD trajectories and two-ion electrostatic potential energy profiles also highlight the importance of the intercation Coulombic repulsion in ion permeation in the acetylcholine receptor.

Acknowledgments This work is supported by funding from the National Health and Medical Research Council of Australia, an award under the merit allocation scheme of the APAC National Facility at the ANU, and additional computer time from iVEC.

References

Ashcroft FM (2006) From molecule to malady. Nature 440:440–447

Auerbach A, Sigurdson W, Chen J, Akk G (1996) Voltage dependence of mouse acetylcholine receptor gating: different charge movements in di-, mono- and unliganded receptors. J Physiol 494:155–170

Barry PH, Lynch JW (2005) Ligand-gated channels. IEEE T NanoBiosci 4:70–80

Beckstein O, Sansom M (2004) The influence of geometry, surface character, and flexibility on the permeation of ions through biological pores. Phys Biol 1:42–52

Beckstein O, Sansom MSP (2006) A hydrophobic gate in an ion channel: the closed state of the nicotinic acetylcholine receptor. Phys Biol 3:147–159

Beckstein O, Biggin PC, Bond P, Bright JN, Domene C, Grottesi A, Holyoake J, Sansom MS (2003) Ion channel gating: insights via molecular simulations. FEBS Lett 555:85–90

Bocquet N, Nury H, Baaden M, Poupon CL, Changeux JP, Delarue M, Corringer PJ (2009) X-ray structure of a pentameric ligand-gated ion channel in an apparently open conformation. Nature 457:111–114

Chabala LD (1992) Voltage dependence of acetylcholine receptor channel gating in rat myoballs. J Gen Physiol 100:729–748

Cheng X, Lu B, Grant B, Law RJ, McCammon JA (2006) Channel opening motion of α7 nicotinic acetylcholine receptor as suggested by normal mode analysis. J Mol Biol 355:310–324

Chung S, Allen T, Hoyles M, Kuyucak S (1999) Permeation of ions across the potassium channel: Brownian dynamics studies. Biophys J 77:2517–2533

Chung SH, Allen TW, Kuyucak S (2002) Conducting-state properties of the KcsA potassium channel from molecular and Brownian dynamics simulations. Biophys J 82:628–645

Corry B (2004) Theoretical conformation of the closed and open states of the acetylcholine receptor channel. Biochim Biophys Acta 1663:2–5

Corry B (2006) An energy-efficient gating mechanism in the acetylcholine receptor channel suggested by molecular and Brownian dynamics. Biophys J 90:799–810

Corry B, Allen TW, Kuyucak S, Chung SH (2001) Mechanisms of permeation and selectivity in calcium channels. Biophys J 80:195–214

Corry B, O'Mara M, Chung SH (2004) Conduction mechanisms of chloride ions in ClC-type channels. Biophys J 86:846–860

Cymes GD, Grosman C (2008) Pore-opening mechanism of the nicotinic acetylcholine receptor evinced by proton transfer. Nat Struct Mol Biol 15:389–396

Darden T, York D, Pedersen L (1993) Particle mesh Ewald: an Nlog(N) method for Ewald sums in large systems. J Chem Phys 98:10089–10092

Essmann U, Perera L, Berkowitz ML, Darden T, Lee H, Pedersen LG (1995) A smooth particle mesh Ewald method. J Chem Phys 103:8577–8593

Grosman C, Auerbach A (2000) Kinetic, mechanistic, and structural aspects of unliganded gating of acetylcholine receptor channels. J Gen Physiol 115:621–635

Hilf RJC, Dutzler R (2008) X-ray structure of a prokaryotic pentameric ligand-gated ion channel. Nature 452:375–380

Hilf RJC, Dutzler R (2009) Structure of a potentially open state of a proton-activated pentameric ligand-gated ion channel. Nature 457:115–119

Hoyles M, Kuyucak S, Chung SH (1998) Solutions of Poisson's equation in channel-like geometries. Comput Phys Commun 115:45–68

Hummer G, Rasaiah JC, Noworyta JP (2001) Water conduction through the hydrophobic channel of a carbon nanotube. Nature 414:188–190

Jackson MB (1986) Kinetics of unliganded acetylcholine receptor channel gating. Biophys J 49:663–672

Jordan PC (2005) Fifty years of progress in ion channel research. IEEE T NanoBiosci 4:3–9

Law RJ, Henchman RH, McCammon JA (2005) A gating mechanism proposed from a simulation of a human α7 nicotinic acetylcholine receptor. Proc Natl Acad Sci USA 102:6813–6818

Leibowitz MD, Dionne VE (1984) Single-channel acetylcholine receptor kinetics. Biophys J 45:153–163

Li SC, Hoyles M, Kuyucak S, Chung SH (1998) Brownian dynamics study of ion transport in the vestibule of membrane channels. Biophys J 74:37–47

Liu X, Xu Y, Li H, Wang X, Jiang H, Barrantes FJ (2008) Mechanics of channel gating of the nicotinic acetylcholine receptor. PLoS Comput Biol 4:e19

Liu Y, Dilger JP (1991) Opening rate of acetylcholine receptor channels. Biophys J 60:424–432

MacKerell Jr AD, Bashford D, Bellott M, Dunbrack Jr RL, Evanseck JD, Field MJ, Fischer S, Gao J, Guo H, Ha S, Joseph-McCarthy D, Kuchnir L, Kuczera K, Lau FTK, Mattos C, Michnick S, Ngo T, Nguyen DT, Prodhom B, Reiher III WE, Roux B, Schlenkrich M, Smith JC, Stote R, Straub J, Watanabe M, Wiórkiewicz-Kuczera J, Yin D, Karplus M (1998) All-atom empirical potential for molecular modelling and dynamics studies of proteins. J Phys Chem B 102:3586–3616

Magleby KL, Stevens CF (1972) The effect of voltage on the time course of end-plate currents. J Physiol 223:151–171

Miyazawa A, Fujiyoshi Y, Unwin N (2003) Structure and gating mechanism of the acetylcholine receptor pore. Nature 423:949–955

Ng JA, Vora T, Krishnamurthy V, Chung SH (2008) Estimating the dielectric constant of the channel protein and pore. Eur Biophys J 37:213–222

O'Mara M, Cromer B, Parker M, Chung SH (2005) Homology model of the $GABA_A$ receptor examined using Brownian dynamics. Biophys J 88:3286–3299

Pascual J, Karlin A (1998) State-dependent accessibility and electrostatic potential in the channel of the acetylcholine receptor: inferences from rates of reaction of thiosulfonates with substituted cysteines in the M2 segment of the α subunit. J Gen Physiol 111:717–739

Phillips JC, Braun R, Wang W, Gumbart J, Tajkhorshid E, Villa E, Chipot C, Skeel RD, Kale L, Schulten K (2005) Scalable molecular dynamics with NAMD. J Comput Chem 26:1781–1802

Sheridan RE, Lester HA (1977) Rates and equilibria at the acetylcholine receptor of electrophorus electroplaques. J Gen Physiol 70:187–219

Sine SM, Engel AG (2006) Recent advances in Cys-loop receptor structure and function. Nature 440:448–455

Sotomayor M, Vasquez V, Perozo E, Schulten K (2007) Ion conduction through MscS as determined by electrophysiology and simulation. Biophys J 92:886–902

Spronk SA, Elmore DE, Dougherty DA (2006) Voltage-dependent hydration and conduction properties of the hydrophobic pore of the mechanosensitive channel of small conductance. Biophys J 90:3555–3569

Taly A, Delarue M, Grutter T, Nilges M, Novère NL, Corringer PJ, Changeux JP (2005) Normal mode analysis suggests a quaternary twist model for the nicotinic receptor gating mechanism. Biophys J 88:3954–3965

Unwin N (1995) Acetylcholine receptor channel imaged in the open state. Nature 373:37–43

Unwin N (2003) Structure and action of the nicotinic acetylcholine receptor explored by electron microscopy. FEBS Lett 555:91–95

Unwin N (2005) Refined structure of the nicotinic acetylcholine receptor at 4 Å resolution. J Mol Biol 346:967–989

Wang HL, Cheng X, Taylor P, McCammon JA, Sine SM (2008) Control of cation permeation through the nicotinic receptor channel. PLoS Comput Biol 4:e41

Wilson GG, Karlin A (1998) The location of the gate in the acetylcholine receptor channel. Neuron 20:1269–1281